Refined Sr_2FeMoO_6 interface realized with photoemission and magnetization analysis

I. Angervo[a,], M. Saloaro[a,], S Granroth[b], H. Huhtinen[a], P. Paturi[a]

[a] *Wihuri Physical Laboratory, Department of Physics and Astronomy, FI-20014 University of Turku, Finland*
[b] *Materials Research Laboratory, Department of Physics and Astronomy, FI-20014 University of Turku, Finland*

Abstract

We investigate the effects of *ex situ* post-annealing on a set of identically deposited Sr_2FeMoO_6 (SFMO) thin films. The annealing provides a significant enhancement to ferrimagnetic exchange, evidenced by almost 40 K increase in Curie temperature. The electronic nature of the film surface is our focus of interest. The detailed analysis on oxygen 1s, strontium 3d, molybdenum 3d spectrum along with changes in the carbon contamination show purification from additional phases and significant valence fluctuation. Successful *ex situ* treatment provides films with higher Curie temperature and diminished surface contamination. Annealing therefore provides a possible method of reobtaining a portion of the valuable bulk attributes at interfaces in e.g. spin valve structures.

Keywords: Sr_2FeMoO_6, thin film, *ex situ*, X-ray photoelectron spectroscopy

1. Introduction

The double perovskite oxides exhibiting a strong magnetoresistive response have great potential in future spintronic applications. Sr_2FeMoO_6 is a material, which combines magnetoresistive phenomenon, linked to spin-polarization of carrier electrons, to high Curie temperature above room temperature [1]. SFMO films tend to easily loose some of their attractive properties compared with bulk samples. This includes, for example, a decreased

Email address: ijange@utu.fi (I. Angervo)

temperature for ferro-paramagnetic transition and diminished phase purity [2–4]. An optimal film fabrication would be a crucial improvement regarding the reduced quality in the films. This means either optimization in the *in situ* film fabrication or a succesfull *ex situ* annealing enhancing the desired attributes and increased understanding about the intrinsic magnetic phenomena in the material. While the intrinsic properties are undoubtedly important, promising attributes can be subdued in multilayer devices by unfavorable interface properties. This points interest towards the surface structure and chemical analysis of the film surface. Earlier, we have characterized SFMO surface structure regarding the surface roughness [5] but we have not studied the electronic structure. However, previous studies by other groups have contributed to the electronic structure of SFMO [2, 6–8].

The analysis of electronic structures in SFMO has been particularly focused on Fe and Mo valence states because of their immediate role in magnetic properties [6, 7, 9]. It has been shown that SFMO is accompanied by both valence states Fe^{2+} and Fe^{3+} [6, 7] resulting with degenerate Fe^{2+}-Mo^{6+} and Fe^{3+}-Mo^{5+} valence both leading to ferrimagnetic orientation between Mo and Fe sublattices. The valence fluctuation between Fe^{2+} and Fe^{3+} can be linked to oxygen vacancies [9] and can also develope an exchange interaction, Fe^{3+}-O-Mo-O-Fe^{2+}, with itinerant electrons [10]. Sr valence has also been reported and used to argue the possible presence of additional phases [2, 8]. However, the role of surface electronic structure as an attractive interface for multilayers is still unclear.

In this work, we investigate the effects of high vacuum annealing on a set of identically deposited SFMO thin films. Our research consists of structural and magnetic characterization. The focus, however, is given to surface analysis performed with surface sensitive X-ray photoelectron spectroscopy (XPS), a technique providing information on electronic structure in SFMO films.

2. Experimental details

Four identical SFMO thin films were prepared with pulsed laser deposition (PLD) on $SrTiO_3$ (100) single crystal substrates. The deposition was conducted at the temperature of 1050°C in 9 Pa Ar-atmosphere. Deposition temperature used here is somewhat higher from what has been occasionally used for fabrication of SFMO thin films with PLD [13, 14]. However, the used deposition temperature here is well within what has been obtained

from our previous optimization [4, 11, 12]. The thickness was controlled with the number of laser pulses and all films were prepared with 2000 pulses. This has previously been shown to equal approximately 120 nm thickness in the films [5, 15]. The *ex situ* annealing was conducted in an ultra high vacuum chamber connected to X-ray photoelectron spectroscopy setup. Treatment for one sample involved increasing the temperature from the room temperature to 200°C (T200), 400°C (T400) or 550°C (T550) with the rate of 10°C per minute. The annealing temperature was maintained for an hour and finally temperature was decreased with the same rate to ambient temperature. One of the samples (T25) was simply stored in the measurement chamber to deduct the possible effects arising only from the ultra high vacuum.

Sample quality was checked with X-ray diffraction (XRD) using Empyrean diffractometer with five axis goniometer and Cu Kα radiation. $\theta - 2\theta$-measurements between $20° - 110°$ were conducted to ensure phase purity of the films. $\phi - \psi-$measurements were done for SFMO (204)-peak ($2\theta = 57.106°$) to confirm fully texturized and $c-$axis oriented SFMO phase. For a more inclusive impurity analysis, $\phi - \psi-$measurements were carried out for possible impurity phases including Fe (110) ($2\theta = 44.98°$) and $SrMoO_4$ (112) ($2\theta = 27.68°$). High resolution $2\theta - \phi$ scans were taken from SFMO (204)-peak, used in the texture analysis.

The zero field cooled (ZFC) and field cooled (FC) magnetizations were measured between 10 K and 400 K in the field of 100 mT. The Curie temperature (T_C) was determined as the temperature corresponding to the minimum of the first order derivative in the FC magnetization. Magnetic hysteresis loops were measured between ±500 mT at 10 K and 400 K. The saturation magnetization was defined as the magnetization value in 400 mT magnetic field at 10 K. Magnetic measurements were done using a Quantum Design MPMS SQUID magnetometer.

X-ray photoelectron spectroscopy measurements, before and after the annealing, were performed in ultra high vacuum with Perkin-Elmer PHI 5400 using Mg Kα (1253.6 eV) X-ray radiation and pass energy of 35 eV. We used C 1s peak (284.8 eV) as a standard for binding energy calibration. Every characterization technique was utilized both before and after the annealing. The annealing took place immediately after the first XPS measurement and the second XPS measurement was performed immediately after the annealing without exposing the sample into room atmosphere.

Complementary hard X-ray photoelectron spectroscopy (HAXPES) measurements were obtained in HIKE end-station of the KMC-1 beamline in

BESSY II. The results were obtained for a separate SFMO film prepared with PLD at 950°C temperature on Nb doped $SrTiO_3$ substrate otherwise like described before.

3. Results

3.1. Basic structural characterization

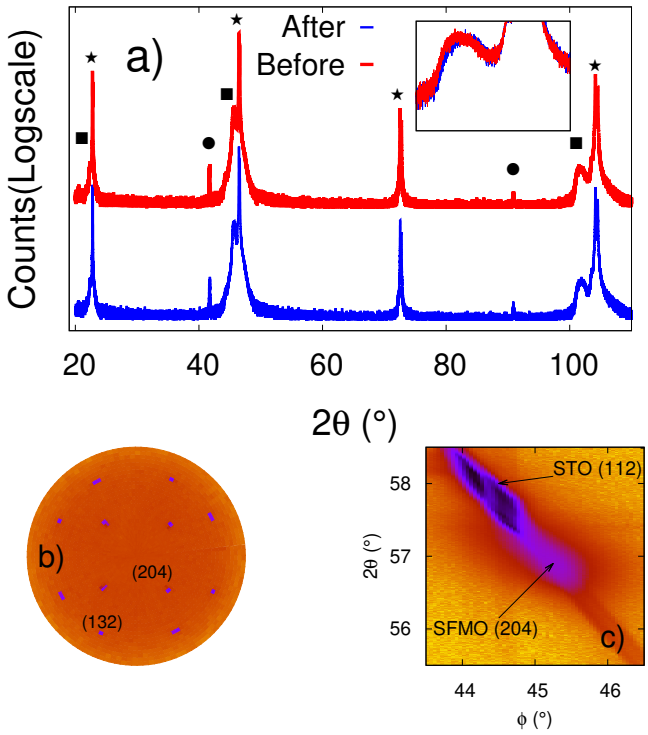

Figure 1: Example of $\theta - 2\theta-$measurement (a), before and after the annealing, and SFMO $\phi - \psi-$results (b), after the annealing, obtained for T550, annealed at the highest temperature. $(00l)$ peaks in $\theta - 2\theta-$results are indicated with a star (★) and square (■) for STO and SFMO, respectively. Peaks arising from K_β radiation are labeled with circle •. An example of $2\theta - \phi-$results of SFMO (204) is presented in c), showing both STO and SFMO peaks. The data presented in (c) was obtained after the annealing.

X-ray diffraction measurements were used to ensure the phase purity and the texturization of the films before and after the annealing. Figure 1 (a)

shows $\theta - 2\theta-$results for the sample annealed at the highest temperature (T550) before and after the annealing and (b) shows $\phi - \psi-$results after the annealing. $\theta - 2\theta-$results show clear signal arising from $(00l)$ planes in the substrate and SFMO. $(00l)$ peaks from STO and SFMO are indicated with a star (★) and a square (■), respectively. Peaks arising from K_β radiation are labeled with a circle •. $\theta - 2\theta-$results can be explained with phase pure STO and SFMO $(00l)$ peaks. A close up on SFMO (008) is presented in the inset of Figure 1 (a) showing no crucial differences between the two scans. $\phi - \psi-$results show symmetrical peaks arising from fully texturized phase. The proximity of the STO peak is imminent with SFMO (204) peak as is seen in Figure 1 (c), presenting an example of $2\theta - \phi-$results obtained for T550 after the annealing. Therefore a portion of the diffraction is due to the substrate material in the $\phi - \psi-$results. However, SFMO (204) signal is clear and any untextured phase should be visible in $\phi - \psi-$results. The XRD results for all the samples confirm that PLD fabrication has produced phase pure, fully textured and c-axis oriented (c-axis parallel with the film in-plane normal) SFMO thin films. Also, no changes were observed between the measurements carried out before and after the annealing. Therefore, none of the *ex situ* treatments, used in this project, does have an effect on phase purity, texture or c-axis orientation in the films. These conclusions are valid within the XRD detection limit of 1% of total sample volume. Although the annealing apparently results with no-significant structural changes, more subtle alterations are likely to take place.

3.2. Magnetic measurements

Since SFMO is considered especially valuable due to its magnetic properties, the effects of the annealing treatment on SFMO films were also monitored with magnetic measurements. Figure 2 (a) presents the ZFC- and FC-measurement results (main panel) for T550, before and after the *ex situ* annealing treatment, along with the first order derivative of the FC-magnetization (inset) used to define T_C. ZFC/FC measurements show the similar tendency between magnetization and temperature as has been reported before [4, 16] without notable differences between the samples in measurements conducted before the annealing. The results for T_C are presented collectively for all the samples in Figure 2 (c). The first measurements, conducted before the annealing, confirm equivalent T_C values, between 310 K and 314 K, for all our samples. All the samples show an increase in T_C after the *ex situ* treatment. The increase in T_C becomes larger with the increasing annealing temperature.

However, for T25 and T200 the increase is insignificant. T_C surged from 314 K to 351 K for T550. When compared with our previously published results, the range of T_C values here are close to the lowest and to the highest values in our preceding reports [4, 11, 12, 15]. However, the method of determining the Curie temperature varies between studies. The highest T_C value is still roughly from 50 to 60 degrees lower, when compared to the reported values for polycrystalline bulk powder samples with T_C of approximately 415 K [1]. The Curie temperature is linked to exchange interaction between Mo and Fe lattice states and it has been shown that an increase of oxygen vacancy concentration can result with an increase in Curie temperature [9, 17].

Saturation magnetization, M_{sat} was determined from the magnetic hysteresis loops. An example of hysteresis loops is presented in Figure 2 (b), again obtained from T550 film before and after the *ex situ* treatment. The hysteresis loops for T550 show that the annealing results with a decrease in saturation magnetization and an increase in coercivity. M_{sat} values, before and after the *ex situ* treatment, are shown in Figure 2 (d) for all the samples. The values for M_{sat} varied from 2.18 μ_B/f.u to 2.29 μ_B/f.u before the annealing. The M_{sat} values after the annealing show that in addition to the Curie temperature also the saturation magnetization is affected by the annealing. Again, T550 shows the most significant change, a decrease from 2.29 μ_B/f.u to 1.92 μ_B/f.u, in M_{sat}. However, not all the samples show a decrease in M_{sat}. Instead T25 and T200 show a slight increase in M_{sat}, while T400 remains essentially unchanged. Like the T_C values, M_{sat} values are also within the range of our previously published results [4, 11, 12, 15] although approximately half from the theoretical maximum value and from the reported experimental values for polycrystalline ceramic samples [1, 18]. The combination of decreasing T_C and increasing M_{sat} is affected by the microstructural lattice defects, anti-site disorder (ASD) and oxygen vacancies. Particularly, oxygen vacancies have been shown to both decrease M_{sat} and increase T_C [9, 17]. ASD refers to the misplacement in SFMO lattice where Fe site has been replaced by the Mo and vice versa.

3.3. Characterization for surface element states with soft XPS

All the presented results for detailed XPS measurements are for T550, annealed at the highest temperature. Fitting was performed using the SPANCF curve fitting macro package, as presented in [19, 20] using Igor Pro fitting program, after subtracting the Shirley type background. Figure 3 (a) presents

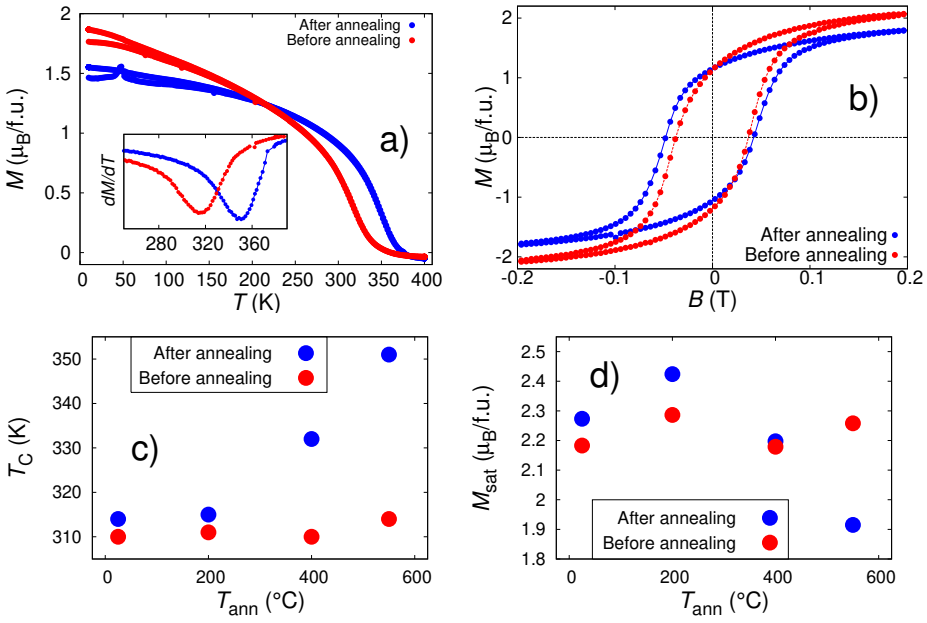

Figure 2: ZFC/FC magnetization measurement (a) and magnetic hysteresis measurement (b) are presented for T550. T_C (c) and M_{sat} (d) are presented for all samples before (red •) and after (blue •) the annealing as a function of annealing temperature.

the survey spectrum for T550 between 1100 eV and 0 eV. The notable features originate from Sr, Fe, Mo and O states along with carbon and are labeled in Figure 3 (a) and (b). Figure 3 (b) highlights the photoemission spectra between 293 eV and 262 eV used in the XPS analysis. This binding energy range provides clear photoelectron signals arising from C 1s and Sr 3p. High vacuum temperature annealing at 550°C diminishes C 1s intensity when compared with Sr 3p peaks. This is probably a result from the vaporization of organic compounds at high temperature. This effect notably takes place in T400 and T550. The annealing also results with an apparent shift in Sr 3p spectra. However, instead of a shift in binding energy, this result most likely comes from a decrease and from an increase in peak intensity between two separate Sr states. This is described in more detail in the following discussion on Sr 3d.

The oxygen O 1s results are presented in Figure 4 (a) and (d) before and after the annealing, respectively. Oxygen can have a profoundly complex 1s

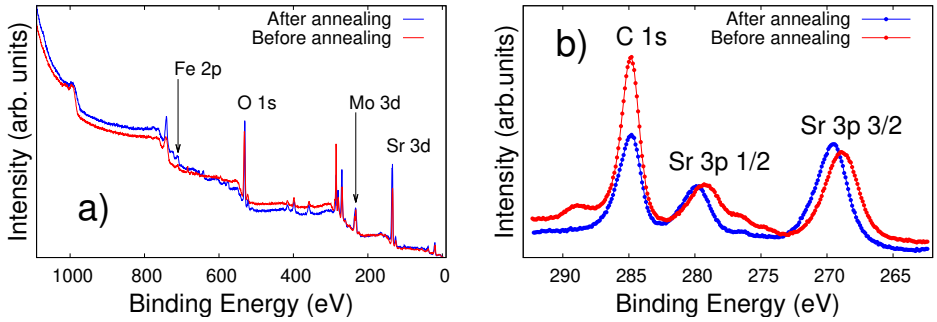

Figure 3: X-ray photoelectron spectra obtained from the energy range between (a) 0 eV and 1100 eV and (b) 293 eV and 262 eV.

photoelectron spectra due to various chemical states falling to a relatively narrow binding energy range. We have used four pseudo-Voigt profiles for all the samples in order to find an explanation for the features in O 1s data. Although an accurate description of the O 1s spectrum would be valuable, this is hampered by the number of possible oxides on the surface originating from SFMO and from separate compounds including oxygen bonds between Fe, Mo, Sr, along from carbon compounds [21]. The annealing clearly diminishes the states in O1 s spectrum at high binding energy. This could well be due to the removal of contaminant hydroxyl and carbonate groups, which have been observed in other perovskites [22–25]. However, the recognized state with the lowest binding energy is also mitigated. The decrease and increase in O1 s relative peak intensities for our other SFMO films after the annealing show tendency towards the results of T550.

The XPS results for molybdenum spectra play an important role in electronic analysis for SFMO films due to the ferrimagnetic orientation between Mo- and Fe-sublattices. Three spin-orbit splitted peak pairs can be identified from the Mo 3d-spectra. An example of the results are presented in Figure 4 (b) and (e) before and after the annealing for T550, respectively. The peaks are attributed to $Mo^{\gamma+}$-(green), Mo^{5+}-(red) and Mo^{6+}-states (blue) [7, 26–30], lower oxidation states corresponding to lower binding energy ($\gamma \leq 4$)[8, 26–28], based on results obtained for Mo-oxides and SFMO. However, Mo 3d-spectra in SFMO and in other compounds has also been explained with more or fewer spin orbit splitted pairs [2, 31]. The separation in binding energy due to spin orbit splitting for Mo 3d was approximately 3.2

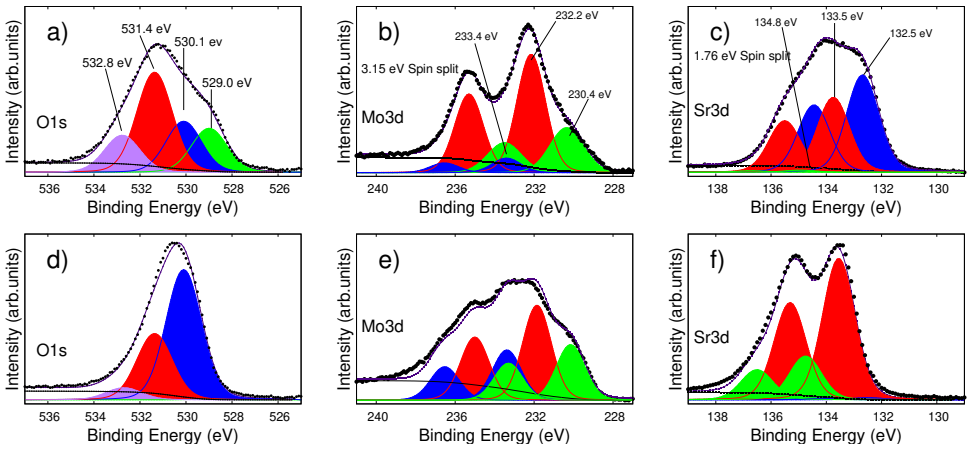

Figure 4: The detailed photoelectron spectra for O 1s, Mo 3d and Sr 3d both before (a, b and c) and after (d, e and f) the annealing. The identified states in Mo 3d contribute to $Mo^{\gamma+}$-(green), Mo^{5+}-(red) and Mo^{6+}-states (blue).

eV. The results obtained for Mo 3d before and after the annealing show significant decrease and increase between relative peak intensities. While Mo^{5+}-states appear as the most dominant part of the data before the annealing, these states become reduced when compared with $Mo^{\gamma+}$- and Mo^{6+}-states after the annealing. Less significant change in relative peak intensities takes place between $Mo^{\gamma+}$- and Mo^{6+}-states as the Mo^{6+}-states become slightly more representative after the annealing. A question can be raised from the identification of the valence states. We would expect $Mo^{\gamma+}$-, Mo^{5+}- and Mo^{6+}-states to appear in the spectrum, lower oxidation with lower binding energy. Based on previous reports we could label Mo^{6+}-state with 232.2 eV binding energy [2, 28, 29]. This would result with unidentified valence at 233.4 eV. Similar problem has been reported for Mo valence states in SFMO [2]. Indeed, the results obtained before the annealing allow the Mo^{6+}-states with the 232.2 eV binding energy value without a clear unidentified valence state. The problem arises in the results after the annealing. According to HAXPES measurements the 232.2 eV binding energy most likely accounts for Mo^{5+}- state.

Figures 4 (c) and (f) show X-ray photoelectron results for strontium 3d binding energy spectra around 135 eV. The results obtained before and after the annealing can be characterized with three separate states. However, one

of the states present in the preliminary results is practically absent from the results obtained after the annealing and vice versa. Two components, due to spin orbit splitting, for one state are separated by approximately 1.8 eV in binding energy. XPS-spectra of Sr 3d in SFMO has been previously explained with three components including the spin orbit split [2, 8]. Even though XPS has been used to study SFMO, the detailed analysis on Sr-components has generally been excluded and the amount of reference appears to be quite limited on SFMO. However, other Sr-compunds, like $SrTiO_3$, have been utilized for Sr 3d characterization, where similar attributes to our investigation can be identified [32–43]. A simple comparison of the binding energy values between previously published results shows that an accurate identification of all the components observed in photoemission spectra can be difficult, since the variation in binding energy values is clear internally and between different reports. Based on the binding energy values, the details in Sr 3d spectra could arise from surface SrO [35, 36, 40], around 133.5 eV ($3d_{5/3}$), from perovskite structure [35, 36, 40], around 132.5 eV ($3d_{5/3}$), and from additional states, around 134.8 eV. For example, the provenance of the additional states could include Sr^{+1} [44] or metallic Sr [45]. However, experiments on Sr compounds have also shown a combination of three states in Sr 3d photoelectron spectra [2, 35, 41, 43] and more reports provide different binding energy values for Sr states [42, 46]. According to HAXPES measurements the peak around 133.5 eV most likely arises from $3d_{5/3}$ and can be attributed to perovskite structure.

3.4. HIKE/HAXPES

HAXPES measurements were conducted on another as-deposited SFMO film fabricated at the temperature of 950°C similarly as reported in [15]. Figure 5 shows results for SFMO electronic structure obtained with 2020 eV and 5000 eV excitation energies. The results were obtained for Mo 3d, O 1s and Sr 3d states. Higher excitation energy provides more bulk relevant response and an argument to support the analysis relating to the electronic structure of SFMO, not the surface contamination.

States in the O 1s binding energy spectrum, both 2020 eV and 5000 eV, show intensity maximum around 530 eV with high energy shoulder as seen in Figure 5 (a). The shoulder becomes reduced when using higher excitation. Molybdenum 3d spectrum provides a clear contribution from Mo $3d^{\gamma+}$, Mo $3d^{5+}$ and Mo $3d^{6+}$ states. The results are shown in Figure 5 (b). 2020 eV spectrum shows a more dominant feature arising from the Mo

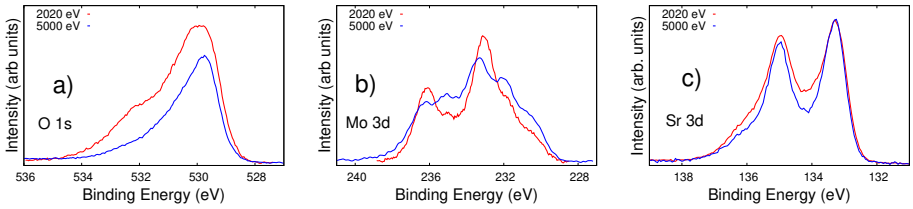

Figure 5: Hard X-ray photoelectron spectroscopy results obtained for O 1s (a), Mo 3d (b) and Sr 3d (c) in HAXPES/HIKE end-station of the KMC-1 beamline in BESSY II.

$3d^{6+}$ spin split doublet. With the higher energy of 5000 eV, $3d^{6+}$ states lose dominance and Mo $3d^{4+}$ and Mo $3d^{5+}$ show increased relative intensity. Mo 3d spectrum obtained from HAXPES measurements is more dominated by Mo $3d^{6+}$ signal compared with the results obtained with laboratory XPS. However, the shift is towards a more mixed valence when higher energy is being used. Actually, the more dominant feature of the Mo $3d^{6+}$ signal in the spectrum was obtained for T400 after the annealing and these results appeared similar to the ones presented for Mo 3d HAXPES results with lower 2020 eV energy. The more mixed valence in the Mo 3d and the reduction of high energy shoulder in O 1s spectrum was seen resulting from the annealing, with the highest temperature, in the XPS measurements. Both, O 1s and Mo 3d, photoemission spectra appear similar to the results obtained with laboratory setup XPS after the annealing.

Figure 5 (c) presents the results obtained for Sr 3d states with HAXPES. No significant difference between 2020 eV and 5000 eV measurements are identified except a slight reduction of the shoulder peak at high energy in 5000 eV measurements and stronger dominance of the spectra by the peak at 133.5 eV and the spin split pair. One noteable detail in Sr 3d spectra obtained with HAXPES is that it lacks the low energy component observed in the measurements for the unannealed SFMO films. Energy spectrum for Sr 3d with both energies in HAXPES measurements show more resemblance with XPS measurements conducted after the annealing. This suggests that the results after the annealing obtained with laboratory XPS are more relevant to the electronic structure of SFMO and do not simply arise from surface contamination.

4. Discussion

This report focuses on investigating the effects of *ex situ* post annealing on the electronic properties of SFMO thin films. The main subjects of the following discussion are illustrated in Figure 6. According to the XRD measurements, SFMO films remain phase pure, fully texturized and c-axis oriented after the annealing. Magnetic properties showed gradual but eventually significant increase in T_{C} between the samples with increasing annealing temperature. M_{sat} shows a more indistinct decrease as a function of increasing annealing temperature. These results confirm that high temperature annealing alters SFMO, at least by possibly inducing oxygen vacancies. Vacuum annealing has been shown to induce oxygen vacancies in SFMO films in previous studies [17]. The electronic structure showed significant changes in the photoelectron spectra before and after the annealing and the results after the annealing are similar to high energy HAXPES measurements.

The electronic structures in photoelectron spectra arise primarily from surface elements, which may well consist of additional phases outside SFMO perovskite or its surface. For this reason, hard X-ray photoelectron spectroscopy measurements were included to give information more relative to the film bulk. The sample used in HAXPES measurements was different, from the annealed samples used in XPS measurements. The fact, that HAXPES measurements conducted with higher X-ray energy, resemble soft XPS results after the annealing, suggests that annealing provides a considerable cleansing from various surface species outside the perovskite structure. This is supported by the demise of carbon and high binding energy oxygen signals in the measurements.

The analysis in the electronic state of SFMO shows an increase in relative intensity towards Mo^{+6} from Mo^{+5}. This could indicate that the degenerate states between Fe^{+2}/Mo^{+6} and Fe^{+3}/Mo^{+5} become more mixed. This could mean that parasitic surface elements, which are removed with the annealing, prefer Mo^{+5} or that SFMO crystal structure on the surface is Mo^{+5} rich and the annealing alters this towards Mo^{+6}. An interesting detail obtained from the annealed samples was that while T550 showed mixed valence from Mo^{+5} dominant spectra towards Mo^{+6} states, T400 showed more dominant features from Mo $^{+6}$ after the annealing when compared to T550. This means that higher annealing has resulted with valence states comparable with the results measured with 5000 eV HAXPES. The role of lattice site augmentation in the electronic state has been reported before [17, 29]. The previous

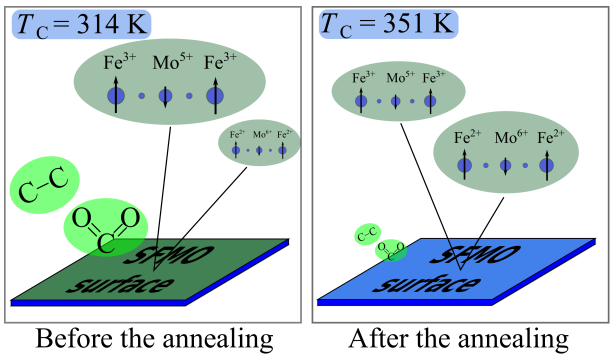

Figure 6: The main contributions resulting from the annealing include removal of the organic impurities, possible fluctuation towards mixed valence between Fe^{2+}-Mo^{6+} and Fe^{3+}-Mo^{5+} and significant surge in Curie temperature.

investigations suggest that the shift in binding energy in O 1s, Sr 3d and Mo 3d spectrum is caused by the oxygen vacancies [17]. Indeed, +0.2 eV shift to higher binding energy would improve the fit for Mo 3d in Figure 4 (e). This requirement, however, is not consistent with O 1s and Sr 3d spectra nor with the results obtained for T400, where, according to our magnetic results, we could expect oxygen vacancies although in lower concentration. In speculative sense crystallographic defects, like oxygen vacancies and ASD, might induce valence fluctuation, which explain our results. Electron doping by the addition of La of the A-site element in the perovskite has been shown to promote the Mo^{+5} state relative to Mo^{+6} state [29] and increase the Curie temperature. This scenario is usually argued through double exchange interaction [47]. A conclusive data for Fe^{+2} and Fe^{+3} valence fluctuation was not obtained with laboratory XPS. With HAXPES, both valence states for Fe^{+2} and Fe^{+3} were obtained from Fe 2p state. This data is planned to be used in report focusing for further HAXPES analysis. The valence fluctuation of states is reported by others for SFMO and identified with spectroscopy techniques [6, 7].

From the elements regarding our analysis, Sr provides especially interesting results. Based on our XPS, HAXPES measurements and additional reports, we can argue that annealing clears additional phases from SFMO surface rather than removes perovskite states. This is because no annealing is involved in HAXPES which could promote the Sr-sites in the SFMO lattice and the Sr 3d state with 132.5 eV binding energy is absent. This means

that 133.5 eV state arises from the perovskite states. Unfortunately, binding energy values from other additional reports would suggest that 132.5 eV states arise from perovskite states and higher 133.5 eV counts for SrO valence states. SrO states would be due to the surface-core-level shift [40]. These assumptions would mean that perovskite states are completely removed after the annealing. This kind of destruction of the lattice signal would indicate a highly mobile Sr segregation resulting with either a perovskite A-site vacancy or with an outcome of secondary phases or significant change in bulk chemical environment. These remarks are down played by the results obtained from our HAXPES measurements and from other reports suggesting other binding energy values for Sr 3d states.

5. Conclusions

We have shown that *ex situ* annealing provides a considerable cleansing for SFMO films from organic compounds. This is clearly seen in the surface characterization for electronic states. The annealing could therefore enhance the interface layer between multilayer sections in e.g. spin valve structures. The electronic states of SFMO are also possibly pushed towards a more mixed valence states between Fe^{+2}/Mo^{+6} and Fe^{+3}/Mo^{+5}. This suggests that SFMO bulk valence states are modified. This conclusion is based on the analysis of Mo 3d spectra. The effects of the annealing on SFMO bulk are clearly seen in the magnetic properties, described by the hysteresis and ZFC/FC-measurements, for example as an increase in the T_C. The annealing appears to provide an improvement to our films without a clear trade-off.

Acknowledgments

The Jenny and Antti Wihuri foundation and the University of Turku Graduate School are acknowledged for financial support. We thank the Helmholtz-Zentrum Berlin - Electron storage ring BESSY II for the allocation of synchrotron radiation beamtime at beamline KMC-1, as well as beamline scientists M. Gorgoi, R. Ovsyannikov and R. F. Duarte. This project has received funding from the European Unions Seventh Framework Programme for research, technological development and demonstration under the NMI3-II Grant number 283883.

References

[1] K. I. Kobayashi, T. Kimura, H. Sawada, K. Terakura, Y. Tokura, Room-temperature magnetoresistance in an oxide material with an ordered double-perovskite structure, Nature 395 (1998) 677.

[2] J. Santiso, A. Figueras, J. Fraxedas, Thin films of Sr_2FeMoO_6 grown by pulsed laser deposition: Preparation and characterization, Surf. Interface Anal. 33 (2002) 676.

[3] A. Venimadhav, F. Sher, J. P. Attfield, M. G. Blamire, Oxygen assisted deposition of Sr_2FeMoO_6 thin films on $SrTiO_3$(100), J. Magn. and Magn. Mater. 269 (2004) 101.

[4] P. Paturi, M. Metsänoja, H. Huhtinen, Optimization of deposition temperature and atmosphere for pulsed laser deposited Sr_2FeMoO_6 thin films, Thin Solid Films 519 (2011) 8047.

[5] I. Angervo, M. Saloaro, J. Tikkanen, H. Huhtinen, P. Paturi, Improving the surface structure of high quality Sr_2FeMoO_6 thin films for multilayer structures., Appl. Surf. Sci. 396 (2017) 754.

[6] J. S. Kang, J. H. Kim, A. Sekiyama, S. Kasai, S. Suga, S. W. Han, K. H. Kim, T. Muro, Y. Saitoh, C. Hwang, C. G. Olson, B. J. P. B. W. Lee, J. H. Shim, J. H. Park, B. I. Min, Bulk-sensitive photoemission spectroscopy of A_2FeMoO_6 double perovskites (a=Sr, Ba), Phys. Rev. B 66.

[7] J. H. Kim, S. C. Wi, S. Yoon, B. J. Suh, J.-S. Kang, S. W. Han, K. H. Kim, A. Sekiyama, S. Kasai, S. Suga, C. Hwang, C. G. Olson, B. J. Park, B. W. Lee, Photoemission and x-ray absorption spectroscopy study of magnetoresistive double perovskite oxides, J. Korean Phys. Soc 43 (2003) 416.

[8] M. Rutkowski, A. J. Hauser, F. Y. Yang, R. Ricciardo, T. Meyer, P. M. Woodward, A. Holcombe, P. A. Morris, L. J. Brillson, X-ray photoemission spectroscopy of Sr_2FeMoO_6 film stoichiometry and valence state, J. Vac. Sci. Technol. A 28 (2010) 1240.

[9] M. Hoffmann, V. N. Antonov, L. V. Bekenov, K. Kokko, W. Hergert, A. Ernst, Variation of magnetic properties of Sr_2FeMoO_6 due to oxygen vacancies, J. Phys. Cond. Mat. 30 (2018) 305801.

[10] T.-Y. Cai, Z.-Y. Li, The effect of the itinerant spin-polarized carriers on magnetization in double-perovskite ferrimagnet Sr_2FeMoO_6, J. Phys. Cond. Mat. 16 (2004) 3737.

[11] M. Saloaro, H. Deniz, H. Huhtinen, H. Palonen, S. Majumdar, P. Paturi, The predominance of substrate induced defects in magnetic properties of Sr_2FeMoO_6 thin films, J. Phys. Cond. Mat. 27 (2015) 386001:1–11.

[12] M. Saloaro, S. Majumdar, H. Huhtinen, P. Paturi, Absence of traditional magnetoresistivity mechanisms in Sr_2FeMoO_6 thin films grown on $SrTiO_3$, MgO and $NdGaO_3$ substrates, J. Phys. Cond. Mat. 24 (2012) 366003.

[13] T. Manako, M. Izumi, Y. Konishi, K.-I. Kobayashi, M. Kawasaki, Y. Tokura, Epitaxial thin films of ordered double perovskite Sr_2FeMoO_6, Appl. Phys. Lett. 74 (1999) 2215.

[14] W. Westerburg, D. Reisinger, G. Jakob, Epitaxy and magnetotransport of Sr_2FeMoO_6, Phys. Rev. B 62 (2000) R767.

[15] I. Angervo, M. Saloaro, , H. Huhtinen, P. Paturi, Interface defects induced vertical magnetic anisotropy in Sr_2FeMoO_6 thin films., Appl. Surf. Sci. 422 (2017) 682.

[16] I. Angervo, M. Saloaro, H. Palonen, S. Majumdar, H. Huhtinen, P. Paturi, Thickness dependent properties of Sr_2FeMoO_6 thin films grown on $SrTiO_3$ and $(LaAlO_3)_{0.3}(Sr_2AlTaO_6)_{0.7}$ substrates, 20th International Conference on Magnetism 75 (2015) 1011.

[17] M. Saloaro, M. Hoffmann, W. A. Adeagbo, S. Granroth, H. Deniz, H. Palonen, H. Huhtinen, S. Majumdar, P. Laukkanen, W. Hergert, A. Ernst, P. Paturi, Toward versatile Sr_2FeMoO_6-based spintronics by exploiting nanoscale defects, ACS Appl. Mater. Interfaces 8 (2016) 20440.

[18] J. Navarro, J. Nogués, J. S. Muñoz, J. Fontcuberta, Antisites and electron-doping effects on the magnetic transition of Sr_2FeMoO_6 double perovskite, Phys. Rev. B 67 (2003) 174416.

[19] E. Kukk, J. D. Bozek, G. Snell, W. T. Cheng, N. Berrah, Vibrational structure and partial rates of resonant auger decay of the N 1s $\rightarrow$ 2 π core excitations in nitric oxide, Phys. Rev. A 63 (2001) 062702.

[20] E. Kukk, K. Ueda, U. Hergenhahn, J. L. X, G. Prumper, H. Yoshida, Y. Tamenori, C. Makochekanwa, T. Tanaka, M. Kitajima, H. Tanaka, Violation of the franck-condon principle due to recoil effects in high energy molecular core-level photoionization, Phys. Rev. Lett. 95 (2005) 133001.

[21] J.-C. Dupin, D. Gonbeau, P. Vinatierb, A. Levasseur, Systematic XPS studies of metal oxides, hydroxides and peroxides, Phys. Chem. Chem. Phys. 2 (2000) 1319.

[22] W. D. Yang, X-ray photoelectron spectroscopy and electrical properties studies of La_2O_3-doped strontium titanate ceramics prepared by sol-precipitation method, J. Mater. Sci 34 (1999) 3533.

[23] M. E. Pilleux, C. R. Grahmann, V. M. Fuenzalida, Hydrothermal strontium titanate films on titanium: An XPS and aes depth-profiling study, J. Am. Ceram. Soc. 77 (1994) 1601.

[24] Y. Zhu, P. A. Salvador, G. S. Rohrer, Controlling the relative areas of photocathodic and photoanodic terraces on the $SrTiO_3$(111) surface, Chem. Mater. 28 (2016) 5155.

[25] W. Jung, H. L. Tuller, Investigation of surface sr segregation in model thin film solid oxide fuel cell perovskite electrodes, Energy Environ. Sci 5 (2010) 5370.

[26] J. Baltrusaitis, B. Mendoza-Sanchez, V. Fernandez, R. Veenstra, N. Dukstiene, A. Roberts, N. Fairley, Generalized molybdenum oxide surface chemical state XPS determination via informed amorphous sample model, Appl. Surf. Sci. 326 (2015) 151.

[27] W. Grünert, A. Y. Stakheev, R. Feldhaus, K. Anders, E. S. Shpiro, K. M. Minachev, Analysis of Mo(3d) XPS spectra of supported Mo catalysts: An alternative approach, J. Phys. Chem. 95 (1991) 1323.

[28] L. Zhang, Q. Zhou, Q. He, T. He, Double-perovskites $A_2FeMoO_{6-\delta}$ (A=Ca, Sr, Ba) as anodes for solid oxide fuel cells, J. Power Sources 195 (2010) 6356.

[29] J. Navarro, J. Fontcuberta, M. Izquierdo, J. Avila, M. C. Asensio, Probing mo core valence on Sr_2FeMoO_6 half-metallic ferromagnets and their electron-doped derivative compounds by photoelectron spectroscopy, Phys. Rev. B 70 (2004) 054423.

[30] K. Kuepper, I. Balasz, H. Hesse, A. Winiarski, K. C. Prince, M. Matteucci, D. Wett, R. Szargan, E. Burzo, M. Neumann, Electronic and magnetic properties of highly ordered Sr_2FeMoO_6, Phys. Stat. Sol. 201 (2004) 3252.

[31] L. V. Kovalev, M. V. Yarmolich, M. L. Petrova, J. Ustarroz, H. A. Terryn, N. A. Kalanda, M. L. Zheludkevich, Double perovskite Sr_2FeMoO_6 films prepared by electrophoretic deposition, ACS Appl. Mater. Inter. 6 (2014) 19201.

[32] V. Young, T. Otagawa, XPS studies on strontium compounds, Applications of Surface Science 20 (1985) 228.

[33] R. P. Vasquez, X-ray photoelectron spectroscopy study of sr and ba compounds, J. Electron. Spectrosc. 56 (1991) 217.

[34] B. Psiuk, J. Szade, K. Szot, $SrTiO_3$ surface modification upon low energy ar^+ bombardment studied by xps, Vacuum 131 (2016) 14.

[35] B. Psiuk, J. Szade, M. Pilch, K. Szot, Xps studies of perovskites surface instability caused by Ar^+ ion and electron bombardment and metal deposition, Vacuum 83 (2009) S69.

[36] D. Petti, R. Bertacco, S. Brivio, M. Cantoni, A. Cattoni, F. Ciccacci, X-ray photoemission study of the $au/la_{0.67}sr_{0.33}mno_3$ interface formation, J. Appl. Phys. 103 (2008) 044903.

[37] R. Bertacco, J. P. Contour, A. Barthélemy, J. Olivier, Evidence for strontium segregation in $La_{0.7}Sr_{0.3}MnO_3$ thin films grown by pulsed laser deposition: consequences for tunnelling junctions, Surf. Sci. 511 (2002) 366.

[38] P. Decorse, E. Quenneville, S. Poulin, M. Meunier, A. Yelon, F. Morin, Chemical and structural characterization of $La_{0.5}Sr_{0.5}MnO_3$ thin films prepared by pulsed-laser deposition, J. Vac. Sci. Technol. A 19 (2001) 910.

[39] H. V. Doveren, J. A. Verhoven, Xps spectra of ca, sr, ba and their oxides, J. Electron. Spectrosc. 21 (1980) 265.

[40] N. B. Brookes, G. Thornton, F. M. Quinn, $SrTiO_3$ step sites as catalytic centers for H_2O dissociation, Solid State Commun. 64 (1987) 383.

[41] K. Szot, W. Speier, U. Breuer, R. Meyer, J. Szade, R. Waser, Formation of micro-crystals on the (100) surface of $SrTiO_3$ at elevated temperatures, Surf. Sci. 460 (2000) 112.

[42] E. O. Filatova, A. A. Sokolov, Y. V. Egorova, A. S. Konashuk, O. Y. Vilkov, M. Gorgoi, A. A. Pavlychev, X-ray spectroscopic study of SrTiOx films with different interlayers, J. Appl. Phys. 113 (2013) 224301.

[43] C. Lenser, A. Koehl, I. Slipukhina, H. Du, M. Patt, V. Feyer, C. M. Schneider, M. Lezaic, R. Waser, R. Dittmann, Formation and movement of cationic defects during forming and resistive switching in $SrTiO_3$ thin film devices, Adv. Funct. Mater. 25 (2015) 6360.

[44] R. Courths, J. Noffke, H. Wern, R. Heise, Photoelectron study of $SrTiO_3$: An inspection of core-level binding energies with the use of a point-ion model and self-consistent atomic-structure calculations, Phys. Rev. B 42 (1990) 9127.

[45] J. C. Fuggle, N. Mårtensson, Core-level binding energies in metals, J. Electron. Spectrosc. 21 (1980) 275.

[46] D. G. Popescu, N. Barrett, C. Chirila, I. Pasuk, M. A. Husanu, Influence of hole depletion and depolarizing field on the $BaTiO_3$ /$La_{0.6}Sr_{0.4}MnO_3$ interface electronic structure revealed by photoelectron spectroscopy and first-principles calculations, Phys. Rev. B 92 (2015) 235442.

[47] J. Navarro, C. Frontera, L. Balcells, B. Martinez, J. Fontcuberta, Raising the Curie temperature in Sr_2FeMoO_6 double perovskite by electron doping, Phys. Rev. B 64 (2001) 092411.